

**AN OPTICAL SET-UP FOR INSPECTING EDGE
CHIPPING DEFECTS OF DWS SOLAR WAFER**

LIM THAI LI

UNIVERSITI SAINS MALAYSIA

2019

**AN OPTICAL SET-UP FOR INSPECTING EDGE CHIPPING DEFECTS OF DWS
SOLAR WAFER**

by

LIM THAILI

**Thesis submitted in fulfillment of the
requirements for the degree of
Master of Science**

May 2019

ACKNOWLEDGEMENT

There are many people that I would like to express my gratitude to throughout this period of my research, where they were the ones who provided me the supports and guided me well.

First of all, I would like to thank the organization that provides the research grant in supporting this project, which is the Collaborative Research in Engineering Science and Technology (CREST), and the grant scheme that supports this project is grant 304/PELECT/6050264/C121.

Then I would like to express my most sincere appreciation to my supervisor, Professor Mohammad Zaid Abdullah, for giving me the most valuable guidance that I could ever get. I am so grateful that I felt the enthusiasm in him in all stages of this research. He had shown the balance of guidance while allowing me to be independent and be particular on details without compromise. I appreciate all the professional comments and corrections which I learned so much.

Also, I would like to take this opportunity to thank Mr. Goon Koon Yin for open up this opportunity of research. He is the person that is so devoted in technology who has motivates me so much throughout these years.

Furthermore, I would like to thanks Teow Wee for all the works that we did together. We had a lot of discussion and idea sharings, especially in our publication paper.

Finally, I would like to extend my warmest regards to my parents and my family members for their support in my decisions. Thanks for care, the encouragement and believing in me for these years.

Last but not least, I would like to thank all whoever helped in making this thesis a success and I'm sorry if I forgot to mention anyone.

Lim Thai Li 2019

TABLE OF CONTENTS

	Page
ACKNOWLEDGEMENT	ii
TABLE OF CONTENTS	iv
LIST OF TABLES	viii
LIST OF FIGURES	ix
LIST OF ABBREVIATIONS	xv
LIST OF SYMBOLS	xvii
ABSTRAK	xx
ABSTRACT	xxi
CHAPTER ONE: INTRODUCTION	
1.1 Background	1
1.2 Importance of Chipping Inspection System	3
1.3 Problem Statement	4
1.4 Research Objectives	5
1.5 Research Scopes	5
1.6 Thesis Outline	6
CHAPTER TWO: LITERATURE REVIEW	
2.1 Introduction	7
2.2 Wafering Process of Silicon-based Solar Wafer	8
2.3 Physical Appearance of DWS Silicon Wafer	10
2.4 Solar Wafer Chipping	13
2.5 Existing Machine Vision System for Chipping Inspection	15
2.5.1 Market available system by OEM	15
2.5.2 Others proposed method	18
2.5.3 Comparison of existing solution	20
2.6 Possible Machine Vision Technique for Chipping Inspection	21
2.7 Machine Vision Illumination	25
2.7 Summary	27

CHAPTER THREE: THEORY

3.1	Introduction	29
3.2	Digital Camera	29
3.2.1	Types of camera	31
3.2.2	Camera FOV	31
3.2.3	Resolution	32
3.2.4	Acquisition frame rate	33
3.2.5	On-the-fly image acquisition	33
3.3	Optics and Lens	34
3.3.1	Geometrical optics	34
3.3.2	Lenses	35
3.3.3	Circle of Confusion (COC)	38
3.3.4	Lens aperture	39
3.3.5	Depth of Field (DOF)	40
3.4	Illumination	41
3.4.1	Lighting technique	42
3.5	Theoretical Design of the Optical Set-up	43
3.5.1	Optimum camera position	43
3.5.2	Determination of spatial resolution	46
3.5.3	Determination of DOF	48
3.5.4	Camera and lens selection	52
3.5.5	Illumination selection	54
3.5.6	Proposed set-up	56
3.5.7	Expected acquired image	59
3.5.8	Full edge length inspection	61
3.5.9	Complete inspection on all available edges	64
3.5.10	Specification of the proposed system	66
3.6	Summary	68

CHAPTER FOUR: METHODOLOGY

4.1	Introduction	69
4.2	Overall Procedure	69
4.3	Design Verification	70
4.3.1	Optimum angle for camera set-up	70

4.3.2	Choice for best illumination	71
4.4	Setting up the Prototype	73
4.4.1	Camera set-up and lens pairing	73
4.4.2	Prototype approach	74
4.5	Performance Evaluation	74
4.5.1	Speed capability	74
4.5.2	Surface view capability	75
4.6	Detection Performance Analysis	76
4.7	Summary	77
CHAPTER FIVE: RESULT & DISCUSSION		
5.1	Introduction	78
5.2	Verification of the Design	78
5.2.1	Optimum camera set-up	78
5.2.2	Best illumination choice	82
5.3	Prototype Set-up	85
5.3.1	Camera and lens pairing	85
5.3.2	Assembled prototype	88
5.4	Verification of the Prototype's Performance	89
5.4.1	Speed of image acquisition	89
5.4.2	Verification view capability	91
5.5	Inspection Results	93
5.6	Summary of Specification Achievement	97
CHAPTER SIX: CONCLUSION		
6.1	Conclusion	99
6.2	Thesis Contribution	100
6.3	Future Works	101
REFERENCES		103
APPENDICES		108
Appendix A: Specification Sheet of the Selected Hardware		
Appendix B: Defect's Region Segmentation Function Code		
Appendix C: Inspection Result of Proposed Set-up		

LIST OF PUBLICATIONS

LIST OF TABLES

	Page
Table 2.1 Comparison of the existing solutions in terms of their resolutions, in-line application's capability and also types of chippings that can be detected.	20
Table 2.2 Summary of the possible machine vision technique and their challenges for the application of chipping inspection.	24
Table 2.3 Unique features of various illuminations	26
Table 3.1 Specification of the proposed system.	66
Table 5.1 Chipping visibility under different types of camera set-up.	82
Table 5.2 SNR of a DWS wafer surface for different type of illumination settings.	83
Table 5.3 Comparison of the edge transition profiles produce under different types of illumination settings.	84
Table 5.4 Pairing of camera with various x towards lens β and N under the requirements of r and D_{req} .	86
Table 5.5 Specifications of the chosen camera and lens.	87
Table 5.6 Number of acquired images per side of wafer and their corresponding success rate.	90
Table 5.7 Number of vertical pixels representing the three surfaces of a wafer's edge.	91
Table 5.8 Results of chipping inspection by the proposed set-up showing the false negative and the false positive of the segmentation follow by the detection of the defect.	95
Table 5.9 Inspection results of intact sample showing the false positive of the segmentation followed by false detection as chipping defect if there is any.	96
Table 5.10 Specification achievement.	97

LIST OF FIGURES

		Page
Figure 1.1	OM image of an example of chipping at the corner of a wafer.	4
Figure 1.2	Photo of the MWSS wafer at the left compare to a DWS wafer on the right.	4
Figure 2.1	Sequence of operations in the Czochralski method. (Brice & Rudolph, 2007).	8
Figure 2.2	The principle of the multi-wire sawing technique. (Möller, 2004).	9
Figure 2.3	Cutting of the wafer by pushing a brick into a web of wires which are coated with abrasive particles. (Schwinde et al., 2015).	10
Figure 2.4	The photograph of fixed-abrasive wire. (Kondo et al., 2008).	10
Figure 2.5	SEM image of the surface of (a) a slurry-sawn wafer, and (b) a DWS wafer. (Bidiville et al., 2009).	11
Figure 2.6	A photograph of a DWS wafer showing striations of different wavelengths. (Sopori et al., 2016).	12
Figure 2.7	Illustration of the 3 types of chippings: (a) the non-through (b) the through, and (c) the side chipping.	14
Figure 2.8	Appearances of chippings on DWS surfaces with saw-mark lines at different wafers edges.	14
Figure 2.9	Sample images of the (a) the non-through, and (b) the through chipping captured by the GP Solar's inspection system. ("Wafer Inspection with Solarscan-WAF-Q", 2017).	16
Figure 2.10	Sample images of the (a) the non-through, and (b) the through chipping captured by the Tordivel Solar's inspection system. ("Tordivel Solar Wafer Surface Measurement System", 2015).	17

Figure 2.11	Wafer inspection solution offered by STVision with (a) unique camera set-up that circulates around the wafer's edges to obtain (b) an image of wafer's side surface. ("Inspection of Solar Cell Edges (SCE) For Cracks and Chipping", 2015).	18
Figure 2.12	A method to detect side chipping from a stack of wafers proposed by Bockli et al. (2013).	19
Figure 2.13	Wafer inspection system proposed by Kim with (a) a top view line scan camera paired with a hybrid illumination device, and (b) a chipping image captured from the device. (Kim, 2014).	19
Figure 2.14	Illustration of a chipping (center) at the wafer's edge capture by the NIR transmittance set-up.	22
Figure 2.15	Schematic showing the mechanism of a 3D stereo system that matches points from two images to form the height information.	23
Figure 3.1	Photo of a typical industrial grade's digital camera exposing its rectangle-shaped sensor at the center when the lens is detached. ("The HR Series: Details Matter", 2017).	30
Figure 3.2	Illustration of a scene with the same FOV, but with different resolutions: (a) 12×12 , (b) 25×25 , and (c) 99×99 pixel.	32
Figure 3.3	Schematic of the geometry of reflection and refraction of light rays when it travels from one medium to another.	35
Figure 3.4	Schematic showing a thin convex lens that focuses collimated light to a focal point at the focal length distance from the lens.	36
Figure 3.5	Schematic showing the formation of a real image, I of an object, O by a simple lens.	37
Figure 3.6	Schematic showing only the point at focal plane will form a small and sharp circle at the sensor plane, where points at other positions will form a bigger circle called the circle of confusion, COC.	38

Figure 3.7	Schematic showing different aperture of a lens ranging from the largest aperture of $f/2.8$ that allow more incoming light to the smallest aperture of $f/16$ where less light is allowed to pass through. (Mason, “Aperture Priority (AV or A)”).	39
Figure 3.8	Schematic showing the comparison between (top) a larger lens aperture, and (bottom) a smaller aperture, affecting the COC at the image plane.	40
Figure 3.9	Illustration of different set-ups of illumination such as (a) direct bright field, (b) direct dark field, (c) co-axial, (d) dome, and (e) back-lit illumination.	42
Figure 3.10	(a) Cartesian axes representation of the wafer with one bottom surface lying on xy -plane. (b) The cross-sectional area of the wafer with camera positioned at an angle θ with respect to y -axis. (c) The surfaces from the camera’s image.	44
Figure 3.11	The graph of the function $f(\theta) = k(\sin \theta + \cos \theta)$ shows that the area is maximum when the camera is set-up at the angle of 45° .	46
Figure 3.12	Illustration showing the measurement of the image’s vertical spatial resolution when the camera is positioned at an angle θ in such a way.	47
Figure 3.13	Illustration of (a) an edge of a wafer and (b) the cross-sectional view of it showing the position of the camera and the expected DOF.	49
Figure 3.14	Schematic of the surface of interest, R_t and R_s and the required DOF to cover them.	49
Figure 3.15	Schematic diagrams showing the variations in the actual case in the (a) y -axis and (b) z -axis direction.	50
Figure 3.16	The variations in actual practice that would further increase the minimum requirement of the DOF.	50
Figure 3.17	Illustrations showing the variations in the z -axis could be caused by (a), (b) different thicknesses of the conveyor belt or (c) the up and down vibration.	51
Figure 3.18	Variations in actual practice in the y -axis and the z -axis that would further increase the minimum requirement of the DOF.	51

Figure 3.19	(a) A sample of a DWS wafer, with (b) a zoomed-out image from one of its surface's section and (c) its corresponding grey value line profile across the center of the section.	55
Figure 3.20	Schematic diagram showing the usage of different illumination techniques such as: (a) multi-angle, (b) back-lit, and direct light, to achieve the objective of the inspection.	56
Figure 3.21	The three surfaces: - (a) top, (b) side, and (c) bottom at any point of a wafer's edge.	57
Figure 3.22	Schematic diagram of the proposed set-up with (a) the original camera position and (b) the camera in vertical position with addition of a mirror.	58
Figure 3.23	Schematic of the proposed set-up's optical components.	58
Figure 3.24	Schematic diagram showing the formation of the image (a) under the use of 2 beam splitters positioned at a section of the wafer's edge, and (b) its cross sectional area of light path.	59
Figure 3.25	Illustration showing separate sections of the generation of image under the proposed set-up.	60
Figure 3.26	Illustration showing the final image that will be generated after applying two beam splitters.	61
Figure 3.27	The edge length of wafer, l_e corresponds to its diameter and size, which is d_w and s_w respectively.	61
Figure 3.28	The full length of the wafer's edge to be inspected, represented by l .	62
Figure 3.29	Illustration showing the full length of wafer's edge, l can be completely inspected by multiple captures of images with width of w , including the overlapping of g between images.	63
Figure 3.30	Schematic diagram of the complete set-up comprising of 4 sets of the camera set-up along with the conveyor and a rotating unit.	64

Figure 3.31	Schematic diagram showing the flow of scanning a wafer convey from left to right, where (a) the wafer passing through the first pair of camera with two edges scanned, then (b) a rotating unit rotates it 90°, and (c) another pair of camera scan the other two edges.	65
Figure 4.1	Flow chart of the approach of this research.	70
Figure 4.2	Illustration of 3 camera set-ups: (a) 0°, (b) 90°, and (c) 45°, in the experiment for comparison.	71
Figure 4.3	Illustration of the definition of correct, false negative and false positive for the defect region segmentation.	77
Figure 5.1	Experimental result of top-view camera with (a) its camera position capturing different types of chippings, (a) a non-through (b) a through, and (c) a side chipping, and (e), (f) and (g) are images after segmentation of (b), (c) and (d) respectively.	79
Figure 5.2	Experimental result of side-view camera with (a) its camera position capturing different types of chippings, (a) a non-through, (b) a through, and (c) a side chipping, and (e), (f) and (g) are images after segmentation of (b), (c) and (d) respectively.	80
Figure 5.3	Experimental result of 45-degree-tilted camera with (a) its camera position capturing different types of chippings, (a) a non-through, (b) a through, and (c) a side chipping, and (e), (f) and (g) are images after segmentation of (b), (c) and (d) respectively.	81
Figure 5.4	Photo of the proposed set-up, showing all major components.	89
Figure 5.5	A full wafer image acquired by 5MP camera.	92
Figure 5.6	The zoomed-out sections of the image showing the top, side and bottom surfaces of the wafer.	92
Figure 5.7	The 5 snaps of images capturing one complete length of a wafer's edge in sequential alignment from left to right shown as (a) to (e) respectively.	93
Figure 5.8	Inspection result for the top surface's non-through chipping where (a) the OM image, (b) the proposed set-up image, (c) the ground truth region and (d) the obtained region.	93

Figure 5.9	Inspection result for the bottom surface's non-through chipping where (a) the OM image, (b) the proposed set-up image, (c) the ground truth region and (d) the obtained region.	94
Figure 5.10	Inspection result for the side chipping where (a) the OM image, (b) the proposed set-up image, (c) the ground truth region and (d) the obtained region	94
Figure 5.11	Inspection result for the through chipping where (a) the OM Image, (b) the proposed set-up image, (c) the ground truth region and (d) the obtained region.	94
Figure 5.12	Inspection result for an intact sample wafer (a) the OM image, (b) the proposed set-up image, (c) the ground truth region and (d) the obtained region	94
Figure A.1	Specification sheet of the selected camera.	109
Figure A.2	Specification sheet of the selected lens.	110
Figure B.1	Function code for region segmentation of defect.	111
Figure C.1	Results of all the 30 defective test samples.	112
Figure C.2	Results of all the 30 intact test samples	113

LIST OF ABBREVIATIONS

3D	3 Dimensional
CCD	Charge-coupled Device
COC	Circle of Confusion
c-Si	Crystalline Silicon
DOF	Depth of Field
DWS	Diamond-Wire Sawn
FOV	Field of View
FPS	Frame per Second
HID	Hybrid Illumination Device
LED	Light Emitting Diode
mono-Si	Mono-crystalline Silicon
MP	Mega Pixel
MWSS	Multi-Wired Slurry Sawn
NIR	Near Infrared
OEM	Original Equipment Manufacturer
OM	Optical Microscope
poly-Si	Poly-crystalline Silicon
PV	Photovoltaic
RGB	Red-Green-Blue
ROI	Region of Interest
SEM	Scanning Electron Microscope
SNR	Signal-to-noise Ratio
TDI	Time Delay and Integration

UPH	Unit per Hour
WD	Working Distance

LIST OF SYMBOLS

μ	Average grey intensity
a	Smallest feature size
c	Permissible circle of confusion
DOF	Depth of field
D_{req}	Depth of field requirement
d_w	Diameter of wafer
$\frac{d}{d\theta}$	Derivative of θ
e	Exposure time
f	Focal length
$f(\theta)$	Function of θ
$f'(\theta)$	First derivative of function $f(\theta)$
$f''(\theta)$	Second derivative of function $f(\theta)$
g	Overlapping between image
g'	Compensated overlapping between image
H	High level of grey value
h_s	Height of side view area on wafer
h'_s	Height of side view area in image
h_t	Height of top view area on wafer
h'_t	Height of top view area in image
I	Time interval
i	Refractive index
i_1	Refractive index of medium 1
i_2	Refractive index of medium 2

k	Constant
k_1	Constant for T1
k_2	Constant for T2
K	Contrast
l	Edge length to be inspect
l_e	Edge length of wafer
L	Low level of grey value
M	Grey value range
n	Number of image frames
N	Aperture F-number
p	Pitch between image frames
q	Smallest feature's pixel mapping
r	Spatial resolution
r_{hor}	Spatial resolution for horizontal axis
r_{ver}	Spatial resolution for vertical axis
R_1	Radius of first lens surface
R_2	Radius of second lens surface
R_s	Side surface of interest
R_t	Top surface of interest
R_c	Camera resolution
S	Side view area on wafer
S'	Side view area in image
S_1	Lens to object distance
S_2	Lens to image distance
s_w	Size of wafer

T	Top view area on wafer
T'	Top view area in image
$T1$	Threshold of level 1
$T2$	Threshold of level 2
V	Velocity
v_s	Variations in side surface
v_t	Variations in top surface
w	FOV width
w_s	Width of side view area on wafer
w_t	Width of top view area on wafer
w'_s	Width of side view area in image
w'_t	Width of top view area in image
x	Pixel size
β	Magnification
θ	Angle
θ_i	Angle of incident ray
θ_r	Angle of reflected ray
θ_t	Angle of transmitted ray
π	Pi
σ	Standard deviation

PENYEDIAAN OPTIK BAGI PEMERIKSAAN KEROSAKAN BUCU WAFER SOLAR DWS

ABSTRAK

Teknik penggergajian wayar berlian (DWS) bagi penghirisan wafer fotovoltaik berkeupayaan untuk menghiris wafer yang lebih nipis pada kadar yang lebih pantas dan juga mengurangkan sisa menggergaji. Namun kadar pemecahan meningkat apabila wafer menjadi semakin nipis. Oleh itu pemeriksaan kecacatan seperti pecahan tepi wafer secara dalam talian menjadi penting. Penyelidikan ini menumpu kepada pembangunan penyediaan optik untuk pemeriksaan pecahan serpihan tepi wafer sekaligus menghasilkan cadangan reka bentuk yang novel. Didapati bahawa sudut optimum untuk kamera adalah pada 45° dan sudut ini menghasilkan keterlihatan permukaan melebihi 70% pada ketiga-tiga permukaan wafer, iaitu permukaan atas, tepi dan bawah. Penggunaan cahaya kubah terbukti efektif dalam menghasilkan kualiti imej yang terbaik untuk permukaan DWS dengan nilai SNR 14.4dB. Iluminasi pencahayaan-belakang dapat menghasilkan kontras paling jelas dengan purata sebanyak 85%. Penyediaan optik yang dicadangkan mampu digunakan dengan penghantar yang berkelajuan 353.7 mm/s, atau bersamaan dengan unit pengeluaran 4200 UPH bagi wafer yang dipisahkan 300 mm antara satu sama lain. Secara keseluruhan sistem ini menghasilkan ketepatan sebanyak 100% bagi pengesanan 3 jenis pecahan tepi iaitu (i) tak menembus, (ii) menembus, dan (iii) serpihan tepi apabila memeriksa sampel tersepih yang bersaiz di antara $33\ \mu\text{m}$ ke $780\ \mu\text{m}$. Skor ketepatan segmentasi kawasan adalah sebanyak 68.1%, manakala kesalahan negatif sebanyak 31.9%, dan kesalahan positif dikekalkan pada 2.3%.

AN OPTICAL SET-UP FOR INSPECTING EDGE CHIPPING DEFECTS OF DWS SOLAR WAFER

ABSTRACT

Diamond-Wire Sawn (DWS) technique in Photovoltaic (PV) wafer slicing has the capability to slice out thinner wafers at a faster speed and lower kerf lost. However, thinner wafers will cause higher breakage rate. In-line inspection of defects such as wafer's edge chipping has become more important. This research focuses on the optical set-up for silicon solar wafer's edge chipping inspection system, resulting in the proposal of a novel set-up. It was discovered that the optimum camera set-up is at 45° and this angular view achieved surface visibility above 70% for all the three surfaces of a wafer's edge, i.e., the top, side, and bottom surfaces. The use of dome light in the set-up was proven effective in generating best image quality for DWS surface with SNR of 14.4dB. Also, the back-lit illumination resulted in the best contrast averaging at 85.0%. The proposed set-up is applicable to run in-line on 353.7 mm/s of conveyer speed, which is equivalent to 4200 UPH production with the wafers pitch of 300 mm per unit. It achieved 100% detection for the three major types of chippings which are (i) the non-through, (ii) the through, and (iii) the side chipping, for chipping samples with size between 33 μm to 780 μm . The correctness of defect region segmentation scores 68.1% with false negative about 31.9% while the false positive maintained at 2.3%.

CHAPTER ONE

INTRODUCTION

1.1 Background

The demand of energy is ever increasing relative to the growth of the world population. Fossil fuels such as coal, oil and gas are still the main source of energy, and with the constant rise of industrialization in the 21st century, energy consumption surges even more. Awareness has arisen that fossil fuels are finite, and will be depleted. Hence, the search for alternative sources is imperative.

A promising alternative source of energy is the renewable energy, for example, solar, wind, tidal and biomass. Among these, Photovoltaic (PV) industry has grown significantly over the past decade due to advancement of technology in recent years. However, the cost to obtain this energy is still high as compared to conventional energy.

Moving towards commercializing the PV system, the manufacturers' aim is always focused on reducing the production cost and increasing the system's energy generation efficiency. Many ongoing researches are looking for improvements throughout the production line.

One way of achieving cost reduction is by slicing out more solar wafers from a single ingot. This implementation sounds very promising where every percent of reduction on wafer's thickness will contribute to the same or even more percent increment of output units. The introduction of The Diamond Wire Sawn (DWS) slicing method makes it achievable as it has the capability in producing thinner

wafers down to only 140 μm in most cases as stated in the “International technology roadmap for photovoltaic (ITRPV) 2017 results” report (2018).

As reported elsewhere, the average wafer breakage during production at the current stage range at 5 – 10% (Rupnowski & Sopori, 2009), and this can be even higher when the wafers are getting thinner. A study carried out by Bidiville et al. (2009) have shown that DWS wafers exhibit lower breakage strength in comparison to Multi-Wire Slurry Sawn (MWSS) wafers. Ironically, thinner wafers with higher breakage rate reduced the final output, and cost might be incurred to improve the handling systems.

The MWSS method has always been the standard wafer slicing method over the past decade (Möller, 2004). However, it was gradually replaced by the DWS method due to the additional advantages in DWS technique of faster slicing and less kerf lost (Kondo et al., 2008).

Various techniques have been introduced since then, such as a coding used for identification marking on solar wafer, known as the Brick Slice Code (BSC). A study by Lanz and Richter (2011) concluded that BSC marked at the edge of wafers up to a depth of 30 μm does not weaken the wafer strength. This can be set as the benchmark in deciding the acceptable size of a chipping defect. In reference to the industrial standard, a few existing in-line inspection systems are capable of detecting chipping defect in the size range of 80 μm to 300 μm (Photovoltaic Test & Automation Solution, 2017, VINESPEC SOLAR, 2017) This will also be considered as a benchmark, where the proposed system should be able to do better with detection limit finer than 80 μm .

As stated in the ITRPV report (“International technology roadmap for photovoltaic (ITRPV) 2016 results”, 2017), DWS of mono-crystalline (mono-Si) silicon has achieved maturity and will be the trend over the coming years, where this method is expected to seize a market share of 90% from 2019 onwards.

1.2 Importance of Chipping Inspection System

A thinner wafer is also more prone to breakage with the existence of defects such as micro-crack and chipping. Kaule et al. (2012) have shown that although there is no obvious crack due to edge contact, the fractures typically propagate from the point of chipping at the edge when the wafer is bent.

Besides improvement in handling thinner wafers, a detection system should be implemented as well. A machine vision inspection is very important in the way to sort out the weak wafers to avoid breakage down the line. It should be applied at critical stages where the earlier it is, the better it is.

The cost of wafer breakage is high, where the direct impact is material cost. Besides that, handling a broken wafer might cost more in terms of machine down time and maintenance. And if the wafer breakage found inside the solar panel is at the final stage, additional resources are required to do the rework.

In regards to the severity of the chipping towards the manufacturing yield, the capability to detect and sort out the defects is equally important when compared to prevention. Figure 1.1 shows an example of a chipping at the corner of a wafer captured by Optical Microscope (OM).

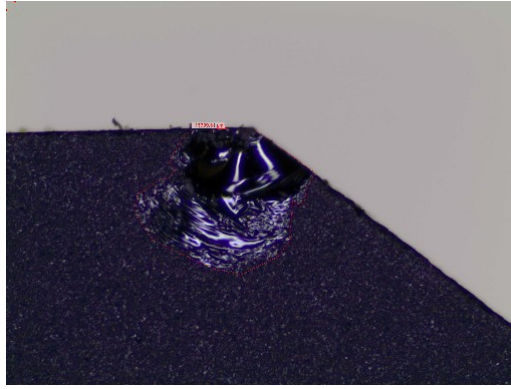


Figure 1.1: OM image of an example of chipping at the corner of a wafer.

1.3 Problem Statement

There are new challenges in visual inspection when dealing with DWS wafers as opposed to MWSS wafers. The visual appearance between MWSS and DWS wafers is very different and this can be observed from the photo shown in Figure 1.2.

The MWSS wafers had smooth and non-glossy surface where defects can be easily spotted. But for a DWS wafer, the visual inspection is very challenging because the surface of such a wafer reflects light in addition to the presence of saw marks and jagged lines as evident from Figure 1.2. Moreover, the brightness deviation is high and thus, making identification of defect extremely difficult.

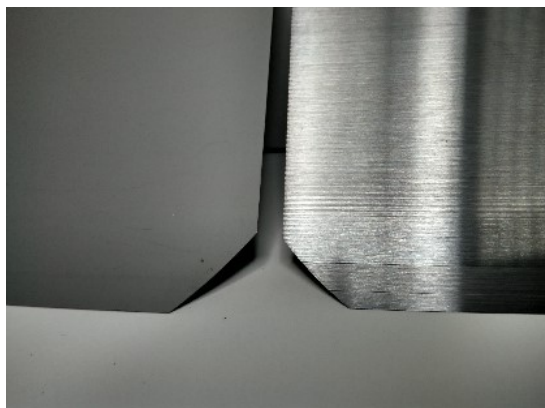


Figure 1.2: Photo of the MWSS wafer at the left compare to a DWS wafer on the right.

The common coverage area inspection for existing in-line systems are on the top and bottom surface of the wafers only. The side surface is mostly ignored since the side chipping does not weaken the wafer especially when it is thick. However, this is not the case for a thinner wafer. Additional set-up to cover the side surface is required, but this will induce an extra cost to the upgrade.

1.4 Research Objectives

The primary objective of this research is to build a machine vision optical set-up of that can perform in-line inspection of chipping defect for the DWS solar wafer. Fulfilling the objective requires the following three secondary objectives. They are:

1. To build a set-up that can perform simultaneous inspection of three surfaces of a wafer's edge, i.e., (i) the top, (ii) the side and (iii) the bottom surface.
2. To develop an inspection system that can detect three major types of chippings. They are (i) the non-through, (ii) the through and (iii) the side chipping.
3. To build a set-up to be applied in-line, with capability of 100% product inspection.

1.5 Research Scopes

The scope of this research is targeted for edge chipping defect's inspection on mono-Si solar wafer that undergoes the DWS wafer slicing process. The Region of Interest (ROI) of the inspection is targeted at the edges of the wafer only where the Field of View (FOV) will be set to 0.2 mm measuring inwards from the edge, with accuracy of 50 μm . Then, the in-line application's capability is limited to

transportation of wafer on a two-belt conveyor system at a total width span of 60 mm at maximum allowable surface vibration of 0.1 mm, and runs at the speed of 300 mm/s which is equivalent to 3600 Unit per Hour (UPH) of wafer's inspection. The target of the inspection is on the edges of the wafer only and the maximum allowable position variation, inclusive of product's size variation is limited to 0.7 mm.

1.6 Thesis Outline

This thesis starts with the first chapter describing the background of the PV industry and DWS technique, followed by the problem faced with thin wafers, and the importance of applying a visual inspection for chipping defects. The second chapter will review the wafering process and characteristics of DWS wafers, types of chipping defects, and the overview of the existing inspection methods. In Chapter 3, theories are given about the optical components (i.e. camera, lens, and illumination), followed by the theoretical design of the proposed set-up.

Chapter 4 provides the methods to verify the design concept, the steps to build a prototype, and approaches taken to analyse the capabilities of the system. Then, in Chapter 5, experiments are carried out, followed by the building of the prototype. Samples of selected defects are tested with the setup and images are obtained for analysis. Finally, in Chapter 6, a general conclusion is provided regarding the study.

CHAPTER TWO

LITERATURE REVIEW

2.1 Introduction

This chapter starts with the introduction of the wafering process in producing the silicon-based solar wafer. A review on the Czocharlski method (Brice & Rudolph, 2007) explains how the silicon crystal was formed, followed by the principle of the multi-wire sawing process. A special focus was done on reviewing the DWS technique for better understanding of its unique features.

Decision on choices of illumination is important for a machine vision system. In order to do that, the physical appearance of the inspecting subject should be studied well. Review was carried out to understand the physical appearance of the DWS wafers surface. The defects in this case which are the chippings are investigated as well.

The literature review will continue on into the existing or market available machine vision system from various Original Equipment Manufacturer (OEM). This study will also include some techniques provided by research papers and patents. Other possible inspection technique such as luminescence imaging, Near Infrared (NIR) transmittance and three-dimensional (3D) vision will be reviewed as well.

Last but not least, the machine vision's illumination will be review, covering various types of lighting such as bright-field, dark-field, diffused, co-axial, dome, and back-lit lighting. And a summary of the reviews will be added to the end of the chapter, added with concise analytical opinions.

2.2 Wafering Process of Silicon-based Solar Wafer

Crystalline silicon (c-Si) is used as the raw material in making the PV solar cell. Two types of commonly used c-Si in producing solar wafers are the mono-Si and the poly-crystalline silicon (poly-Si). The mono-Si wafer is a continuously unbroken crystal without grain boundaries, while poly-Si wafer consists of multiple small silicon crystals which form the visible grain.

Generally, the thin pieces of solar wafers are sliced from silicon ingot, and the ingots are produced from c-Si in various ways. Mono-Si ingots for the solar wafer are mainly produced by the Czochralski method, and the basic steps are shown in Figure 2.1. As described by Brice and Rudolph (2007), the process starts by dipping the seed crystal into the molten silicon. Following that, the action of pulling will take part and rotation is applied simultaneously until the complete cylinder rod of crystal is formed. The molten temperature, rate of pulling and rate of rotation are controlled as they affect the physical shapes of the final product, such as its diameter.

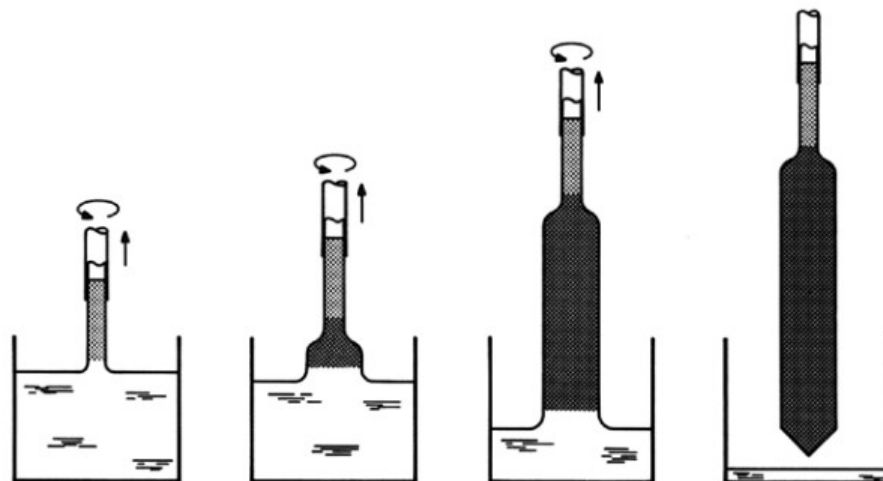


Figure 2.1: Sequence of operations in the Czochralski method. (Brice & Rudolph, 2007)

In the wafering process, the silicon crystals are first cut into bricks of ingot by band saw as explained by Möller (2004). Then, the ingot will undergo the sawing process that cuts it into thin pieces of solar wafers. The principle of the multi-wire sawing technique is depicted in Figure 2.2. A single wire from a supply spool is fed to the wire guides, where the guides contain grooves with constant pitch. Multiple strands of the wire around the guides will form a wire net. One side of the silicon ingot is glued while the opposite side is pushed towards the moving wire net.

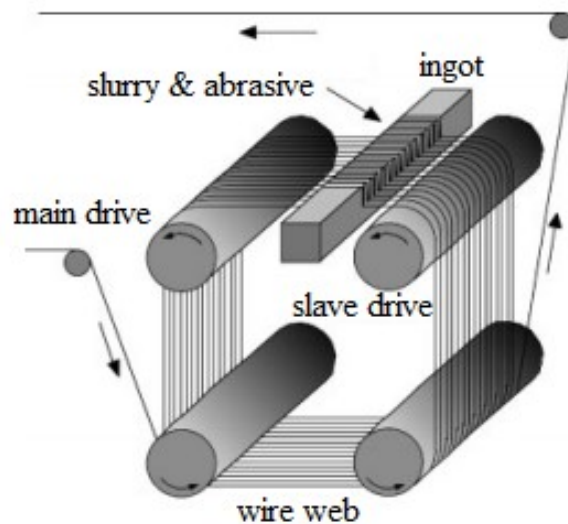


Figure 2.2: The principle of the multi-wire sawing technique. (Möller, 2004)

The moving wires surrounded by abrasive particles works as a saw to abrade away the silicon (Schwinde et al., 2015). As shown in Figure 2.3, the kerf loss is determined by the size of the wire and the particles, but thickness of the wafers are determined by the wire pitches and the kerf. In this process, wastage can be reduced in terms of kerf loss by using thinner wire and smaller abrasive particles. In terms of increasing the wafers quantity per ingot, wire pitch can be reduced to lower down the wafers thickness.

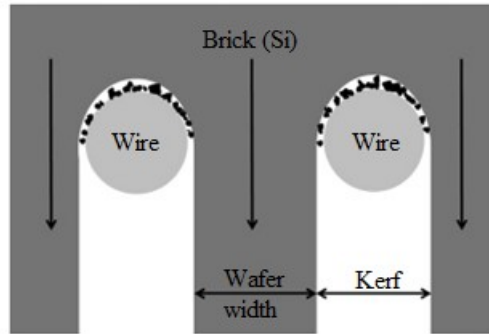


Figure 2.3: Cutting of the wafer by pushing a brick into a web of wires which are coated with abrasive particles. (Schwinde et al., 2015)

For the DWS technique, the sawing wires are coated with abrasive particles as shown in Figure 2.4. As introduced by Kondo et al. (2008), the abrasive particles are fixed to the wire by a type of resin as opposed to the conventional slurry sawing technique that uses loose abrasive particles. Achievement of higher sawing speed was reported when the DWS technique was used.

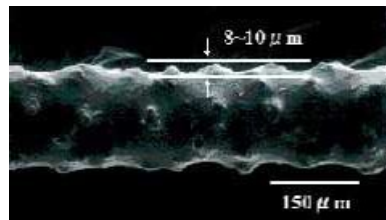


Figure 2.4: The photograph of fixed-abrasive wire. (Kondo et al., 2008)

2.3 Physical Appearance of DWS Silicon Wafer

There is a trend of wafer sawing process shifting from conventional slurry sawing to the DWS sawing technique. As shown previously in Figure 1.2, the appearance of DWS wafer surface is different as well and should be well understood before selecting the illumination.

A study by Hardin et al. (2004) on fixed abrasive diamond wire slicing of silicon wafer reveals that there are formations of scratch grooves on the wafer's

surface. The wires that are used to saw the wafers are coated with diamond grit and these diamond particles that are loose or over protruding on the wire will generate the long stretch groove when the wire moves. These are well described the saw-mark lines with different width parallel to the wire movement direction that exists throughout the whole wafer surface. Recommendation was given to use wires with smaller diamond grit size in order to reduce the surface damage. However, this implementation can only reduce the size of the grooves but will not eliminate it where the saw-mark lines will still be visible.

The introduction of DWS technique is only applicable from the lab to production line if the surface differences of wafers are well explained and updated in the production line. This is the objective from the research from Bidiville et al. (2009) where the statement applies to the inspection process on the wafer. The Scanning Electron Microscope (SEM) image analysis as shown in Figure 2.5 shows that MWSS surface is rough but without the pattern of wire sawing direction. On the contrary, the surface of the DWS wafers contains smooth parallel grooves with slumps of silicon. Visually, the slurry-sawn surfaces are matt-like and texture-less, but the DWS surface contains the texture of saw-mark lines, on the contrary.

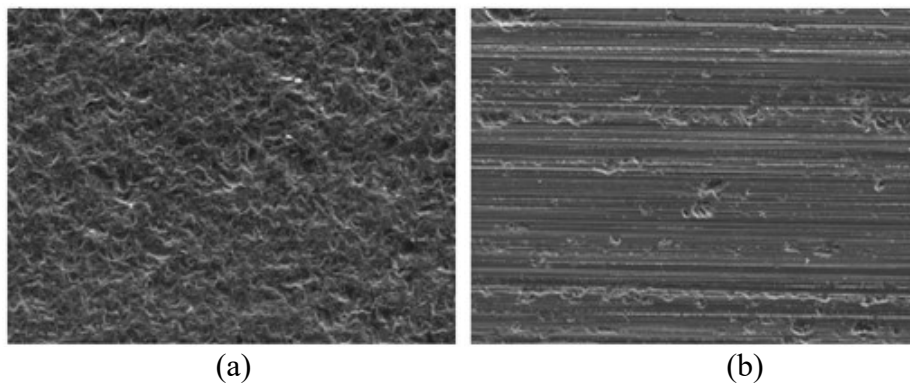


Figure 2.5: SEM image of the surface of (a) a slurry-sawn wafer, and (b) a DWS wafer. (Bidiville et al., 2009)

The surface characteristics of the DWS wafers were also studied by Sopori et al. (2016). Highlighted here is the DWS surface containing striations of varying pitch. The striations with small pitch are mainly due to diamond grit and the step motion of feed mechanism. Then the wire reciprocation and low frequency vibrations are corresponding to the surface height changes in a bigger scale. The photograph of DWS containing striations of different spatial wavelengths can be clearly seen in Figure 2.6. As stated previously, the visibility of the surface features is due to reflectance in the surface height changes.

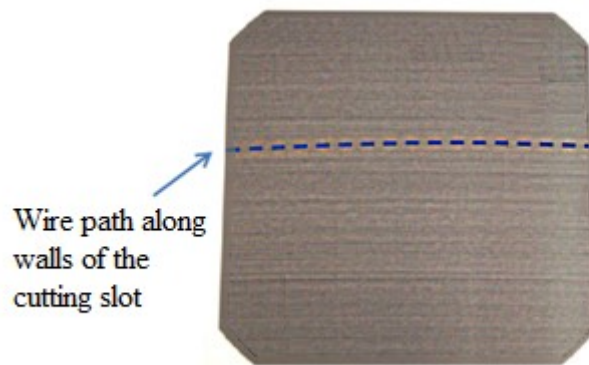


Figure 2.6: A photograph of a DWS wafer showing striations of different wavelengths. (Sopori et al., 2016)

Evidence from research by Teo et al. (2014) has shown that the silicon-based wafers will block visible lights while lights from NIR spectrum will penetrate through it. The intensity of the passed through NIR lights are influenced by the wafer's thickness and also the irradiance strength of the NIR illumination.

The study from Chen et al. (2015) provides useful information about the reflection of the DWS surface compared to slurry-sawn surface. The initial reflection of the DWS surface is 36% while it is 28% for slurry-sawn surface, which means the DWS surface is more reflective. It is believed that the high reflection of the DWS

surface is the visual contrast effect among the shallow and deep grooves where the first one was caused by diamond grits while the later one was caused by direction change of wire reciprocation.

In short, the DWS wafer is a raw silicon material which is grey in colour. The surface contains texture of saw-mark lines in the orientation parallel to wire movement path. The saw-mark lines are different in size, height and also varying in its spatial frequency, sponsoring the visual effect of bright and dark lines and also appeared to be reflective.

2.4 Solar Wafer Chipping

Solar wafer chippings are defects found on the wafer. They are physical defects which occur at the edges of the wafer. Various names such as edge defect, edge fault, edge irregularities, chipping, v-cut, shell chips, flake, crack, break, etc. are given pertaining to these defects. Here in this study, these edge chippings are classified into three categories. Based on their physical appearance and location, they are named as non-through chippings, through chippings and side chippings.

Non-through chippings are materials peel-off from the edge on one side of the wafer surface. It cannot be identified by looking from the other side of the wafer surface. On the other hand, a through chipping is a more severe case with greater loss of material. Indentation can be seen around the wafer outlier from both sides of the wafer surface. Finally, for side chipping, the characteristic is similar to non-through chipping. The only difference is, there is more material loss from the side wall of the wafer's edge.

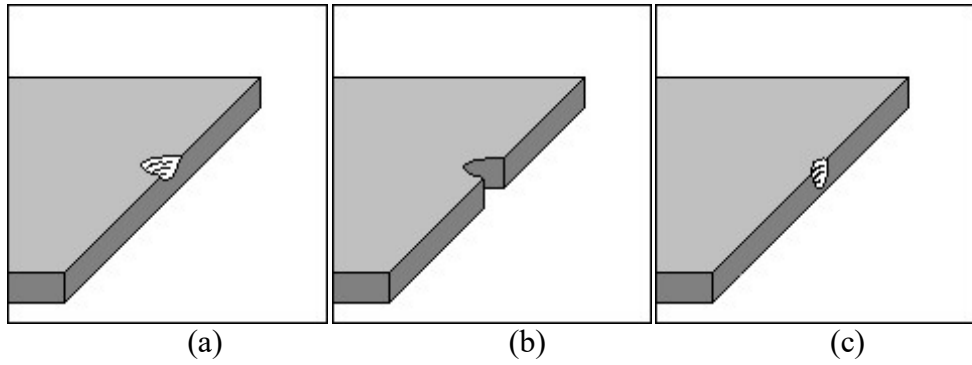


Figure 2.7: Illustration of the 3 types of chippings: (a) the non-through, (b) the through, and (c) the side chipping.

As chipping might occur randomly at any position of the wafers edge, it can be expected that there are mixtures of different saw-mark line patterns at the wafer's edge. Visually, the saw-in edge and the gluing edge of the wafer will have saw-mark lines that are parallel to the edge as illustrated in Figure 2.8. At the left and right edges, the pattern will be perpendicular lines towards the edge. When it comes to chamfer edges, the lines will appear slanted compared to the edge. Care should be given in later parts of illumination set-up and also image processing in order to handle these variations.

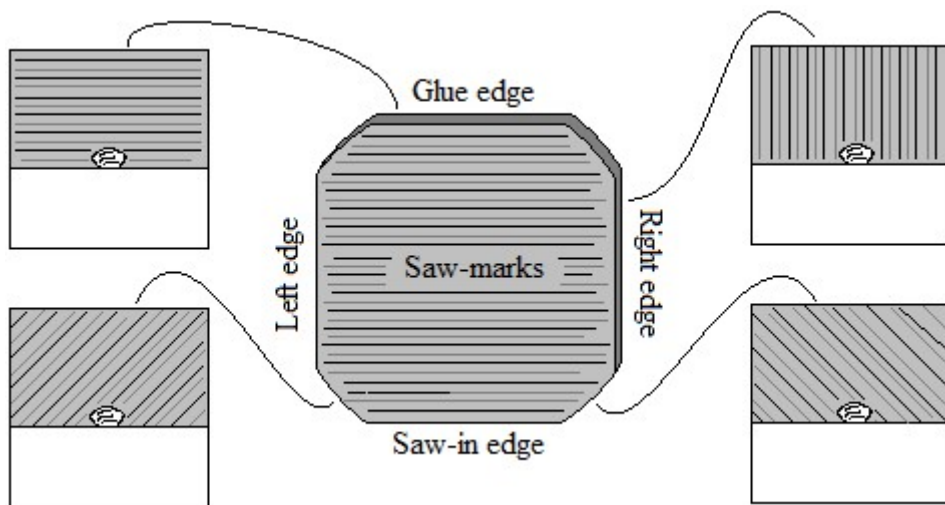


Figure 2.8: Appearances of chippings on DWS surfaces with saw-mark lines at different wafers edges.

2.5 Existing Machine Vision System for Chipping Inspection

Although the visual inspection on solar wafer existed long ago, the process and technique of producing wafer were different then. The system's inspection objectives and capabilities could be different as well.

Basically, there are two types of systems offered, which is quoted as in-line system and offline system here. The in-line system is designed to be deployed to the production lines. Basic capability is to perform high speed 100% inspection. Usually, the speed of the solar wafer production line is 3600 UPH, equivalent to one second per unit. On the other hand, for the offline system, its main focus is to provide high resolution inspection. Normally, it is used as evaluation tools which do not require fast inspection speed.

2.5.1 Market available system by OEM

A common set-up offered by most OEM is the top-view camera set-up, such as the wafer inspection module from GP Solar. Equipped with camera resolution down to 25 μm per pixel, its patented dome technology illumination, and multi-image processing, a few surface defects such as chippings can be identified (“Wafer Inspection with Solarscan-WAF-Q”, 2017). The sample images of chippings are shown in Figure 2.9.

Vitronic, a well-known machine vision systems provider put up an in-line wafer inspection system in its product line (“VINSPEC SOLAR – Optical Wafer and Solar Cell Inspection System”, 2017). This system uses a 4 Mega Pixel (MP) (2048 x 2048) area scan camera overlooking at the wafers' top surface with spatial resolution of 80 μm per pixel. The system covers a few inspection criteria such as edge length measurement, surface defects, unevenness height, cracks, including edge defects.

Stated in the specification, the detection limit of edge defects such as chippings is $170\mu\text{m}$.

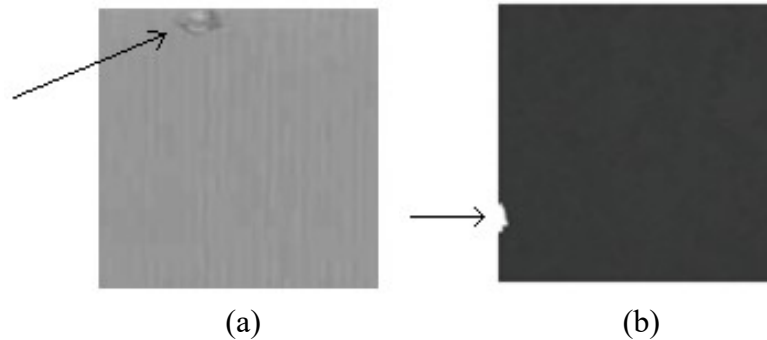


Figure 2.9: Sample images of (a) the non-through, and (b) the through chipping captured by the GP Solar's inspection system. ("Wafer Inspection with Solarscan-WAF-Q", 2017)

Another in-line system offered by Chroma is its capability of running an inspection at the speed of 3000 to 3600 UPH. Under its "Solar wafer geometry and surface inspector", non-through chipping and through chipping will be detected along with the geometry measurement of the solar wafer ("Photovoltaic Test & Automation Solution", 2017). Attached with back lights and surface lights, the FOV of the system captures the full wafer with a detection limit of $80\mu\text{m}$ as stated in its brochure.

Similarly, the "Wafer Surface Measurement System" from Tordivel Solar inspects chippings with a 1280×1024 area scan camera over looking at the surface ("Tordivel Solar Wafer Surface Measurement System", 2015). As shown in Figure 2.10 (a) the non-through chippings appeared as a mixture of dark and bright compared to the wafer surface, while the dark background highlights the outliers of the through chippings as in Figure 2.10 (b). Rough estimation from the camera resolution viewing a 125mm to 156mm full wafer size, the detection resolution is

around $120\mu\text{m}$ to $150\mu\text{m}$. With this low-resolution image, the system is able to do in-line inspection of one second per unit of solar wafer.

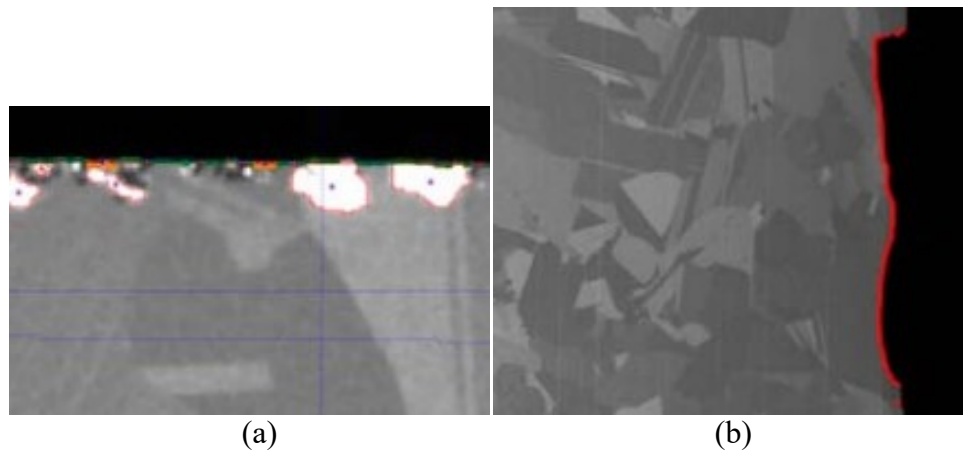


Figure 2.10: Sample images of (a) the non-through chipping, and (b) the through chipping captured by the Tordivel Solar's inspection system. (“Tordivel Solar Wafer Surface Measurement System”, 2015)

Other than that, famous machine visions OEM such as Schmid, Yasunaga and Heneckke also provide such in-line inspection system. Very limited information is disclosed regarding the setup and the capability of their system.

Besides in-line inspection system, STVision presents a standalone inspection system dedicated only for side chipping (“Inspection of Solar Cell Edges (SCE) For Cracks and Chipping”, 2015). Unlike the above-mentioned systems that capture image of top and bottom surface of the wafer, this system capture images of the side of the solar wafer as shown in Figure 2.11. Unique setup of camera and automation enables the scanning to circulate around the wafer that sits on the stage. This system is able to detect chipping as small as $3\mu\text{m}$, but at inspection time of 10 seconds per wafer.

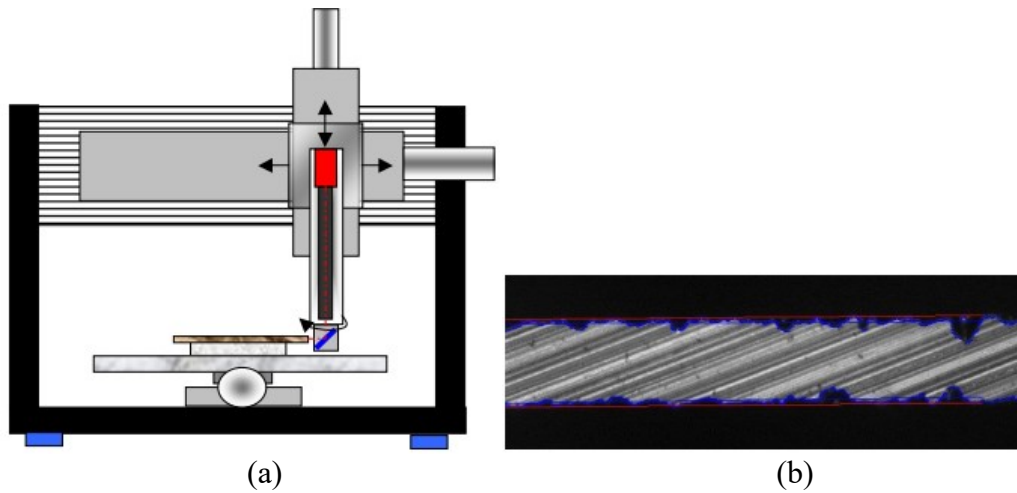


Figure 2.11: Wafer inspection solution offered by STVision with (a) unique camera set-up that circulates around the wafer's edges to obtain (b) an image of wafer's side surface. ("Inspection of Solar Cell Edges (SCE) For Cracks and Chipping", 2015)

The top-view camera set-up in most in-line systems is able to detect through and non-through chippings, but contain blind spots where the side chipping is not detectable. Similarly, a side-view camera set-up that focuses on detecting side chipping is unable to detect chipping at the top and bottom surface.

2.5.2 Others proposed method

The importance of inspecting the side chipping was also highlighted in the paper by Bockli et al. (2013). Similar to the setup of STVision mentioned above, they proposed a standalone system that also captures the side surface of the wafer. However, instead of evaluating the wafers one by one, the system does it in one shot on a stack of wafers. Due to the high magnification and small field of view, multiple captures of images is required to cover one side of the stacked wafers. Undoubtedly, this system is capable of detecting chipping up to a few micro meters in size.

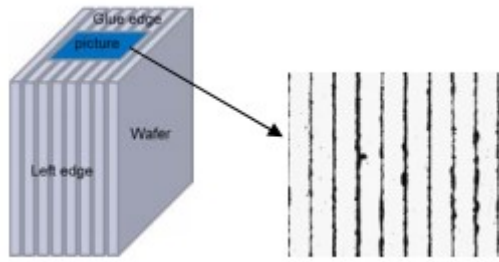


Figure 2.12: A method to detect side chipping from a stack of wafers proposed by Bockli et al. (2013).

Other than that, another system of solar wafer inspection was proposed by Kim (2014). With the target to apply in high speed manufacturing line, and also maintaining the high inspection resolution, a Time Delay and Integration (TDI) line scan camera is used. The pixel size is an impressive $7\mu\text{m}$ per pixel. Equipped with a sophisticated hybrid multi angle light setup, this system is capable of detecting various types of defects including chipping. However, this machine can only view wafer's top surface, while side view is completely left out. This is the major drawback of this inspection system.

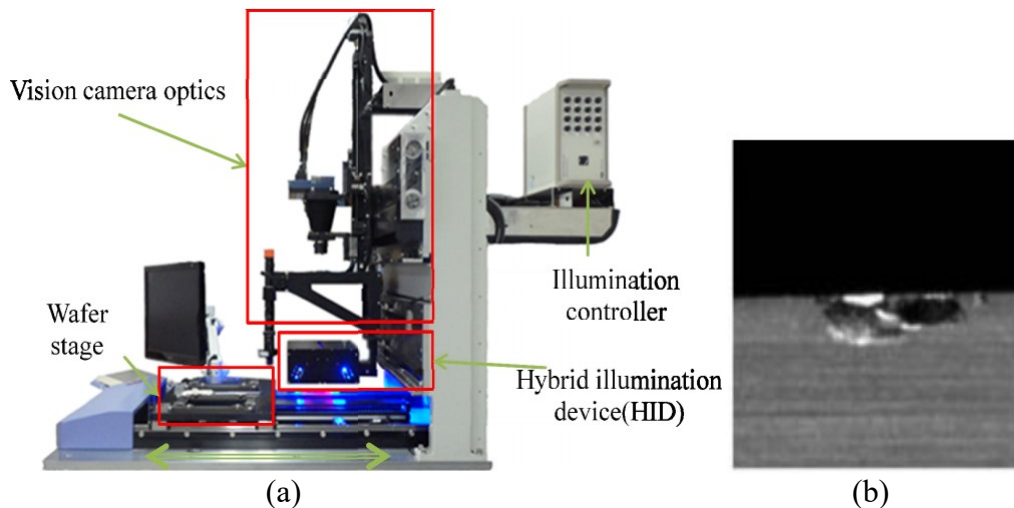


Figure 2.13: Wafer inspection system proposed by Kim with (a) a top view line scan camera paired with a hybrid illumination device, and (b) a chipping image captured from the device. (Kim, 2014)

The edge inspection solution can also be found for semiconductor's wafer. A patented technique by Watkins et al. (2008) combines the set-up of a top-view camera and a side-view camera to inspect both the top and the side surface of the wafer. Additional bottom-view camera can be added as well to cover the bottom surface to give a complete FOV coverage of the edges. However, this is a standalone set-up that only inspects one piece of wafer at a time. Another similar patented set-up was also proposed by Voges et al. (2013).

2.5.3 Comparison of existing solution

The capabilities of each reviewed solutions are summarized and listed in Table 2.1. Highlighted specifications are their system's resolution, types of camera set-up, capability of in-line application, and also types of chipping defects that can be detected.

Table 2.1: Comparison of the existing solutions in terms of their resolutions, in-line application's capability and also types of chippings that can be detected.

Solution provider	Res. (µm)	Camera Set-up Type	In-line / Standalone	Non-Through Chipping Detection	Through Chipping Detection	Side Chipping Detection
GP Solar	25	Top	In-line	✓	✓	×
Vitronic	80	Top	In-line	✓	✓	×
Chroma	80	Top	In-line	✓	✓	×
Tordivel	120	Top	In-line	✓	✓	×
STVision	3	Side	Standalone	×	✓	✓
Bockli	< 40	Side	Standalone	×	✓	✓
Kim	7	Top	In-line	✓	✓	×
Watson	100	Top & Side	Standalone	✓	✓	✓
Voges	n.a.	Top & Side	Standalone	✓	✓	✓

Referring to Table 2.1, clearly all top-view camera set-up systems has blind spot on detecting the side chipping while the side-view camera set-up cannot detect

chippings on the top surface. A combination of these two set-ups can solve the problem. This would inflate the cost of such a system by twofold, because the number of camera, lens and illuminator has to be doubled. Furthermore, the capability of a combined system to be operated inline remains doubtful without major upgrades to the controller hardware.

None of the reviewed systems above has the capability to do a 100% in-line inspection with FOV that can cover the detection of the three major types of chippings stated above.

2.6 Possible Machine Vision Technique for Chipping Inspection

Besides the conventional machine vision set-up in the visible light spectrum range, luminescence imaging has shown its versatility in its application in PV industry for both research and development's works as well as quality measurement in manufacturing line.

The principle of this technique is to make the surface of the subject to be excited and emits luminescence light, and to use a camera to acquire the emission. There are two ways of doing the excitation where one is called Electroluminescence (EL) (Fuyuki et al., 2005; Fuyuki & Kitiyanan, 2008; Tsai et al., 2012) and another one is called Photoluminescence (PL) (McMillan et al., 2010; Trupke et al., 2012).

However, EL requires electrical contact for the excitation and hence it does not work on bare silicon solar wafers (Hinken et al., 2007). Whereas for PL imaging that uses optical excitation, its application is widely used for solar wafers. Lots of researches shows the usability of PL on quality assessment on solar wafers, such as dislocation area fraction, extension of low life-time regions, and others

crystallization-induced material defects. PL proves to have the potential of detecting solar wafer's chipping, but the drawback is its slow acquisition time that can range from 30 to 100 seconds (Trupke et al., 2006; Trupke et al., 2013).

Next, the NIR transmittance setup (Chiou et al., 2011) that is famous for silicon based solar wafer's micro crack detection is also deemed possible in detecting edge chipping. The working principle is the NIR lights are directed from one side of the wafer, and a camera from the other side is use to collect the penetrated light. Impurity defects such as the micro cracks will scatter the incident light, resulting in the formation of dark spot in the image.

One problem of the NIR transmittance technique is the intensity of the penetrating light will be directly affected by the thickness of the solar wafer (Ko et al., 2013; Teo et al., 2014). Due to this, the use of NIR transmittance in detecting wafer chipping is difficult to achieve. Chipping which is the loss of material on wafer surface will appear as a spot of wafer's thickness drop. Stronger penetrating NIR light will be captured and a contrast of brighter spot will be presented in the image as the chipping. Illustration in Figure 2.14 shows the possible outcome of a chipping captured under the NIR transmittance set-up.



Figure 2.14: Illustration of a chipping (center) at the wafer's edge capture by the NIR transmittance set-up.

Besides that, a physical defect such as the chipping can also possibly be detected by a 3D vision system. The stereo 3D system uses two cameras by placing them side by side at a separate distance and viewing a same point of the inspection spot (Ohta & Kanade, 1985). The concept is also applied for set-up with three or more cameras as proposed by Sumi et al. (2002).

The basic mechanism in stereo vision is by matching the pixel from one image to another. As shown in Figure 2.15, the disparity values from each pixel will usually generated into a grey tone image which is called the disparity image, and it provides depth information of height where lighter tones represent nearer, and darker tones represent further away. However, it requires surfaces to have distinct texture in order to do the matching between images.

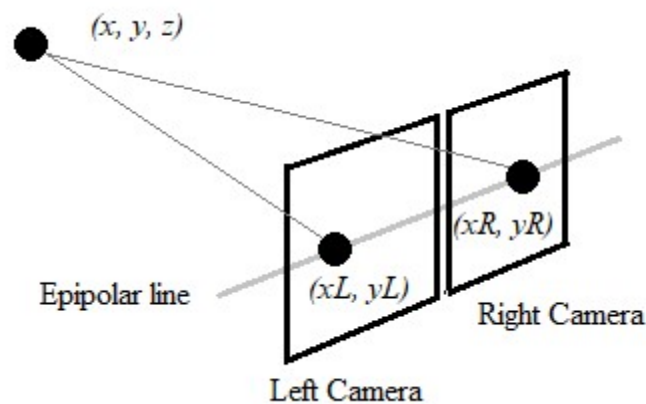


Figure 2.15: Schematic showing the mechanism of a 3D stereo system that matches points from two images to form the height information.

The stereo disparity image matching technique requires consistence intensity from different viewpoints without specular reflection (Sun et al., 2003). This is not suitable for the case of DWS wafer with highly reflective surface. Besides that, the in-line hardware implementation is more complex based on the review done by Lazaros et al. (2008).

Another 3D vision approach that utilizes the triangulation concept is the 3D laser sheet of light system (Acosta et al., 2006; Dorsch et al., 1994). A laser cast a line on the subject, and a line scan camera captures the line. The laser line will appear straight on flat surface but will be offset when coated on uneven surface. Based on the theory, the separation of laser line represents the height different of the surface. A chipping with an indent to the surface could be identified with such system.

On the disadvantages side, Acosta et al. (2006) reported that the laser triangulation sheet of light method suffers from occlusion issue as well as object reflectivity. Also in the current target of DWS wafer, the reflective surface might cause failure for the surface scanning. In addition, comments from Dorsch et al. (1994) stated that speckle from laser will introduce uncertainty using this method. This might require complex algorithm to overcome it.

All the possible techniques mentioned above are summarized into Table 2.2 showing the application of each technique along with the challenges when apply for DWS chipping inspection.

Table 2.2: Summary of the possible machine vision technique and their challenges for the application of chipping inspection.

Possible Technique	Current / Common Application	Challenges of DWS Chipping Inspection
EL	Solar cell inspection	Impossible as it require electrical contact.
PL	Dislocation density; Life time measurement	Slow for as-cut wafer. (30s to 100s).
NIR	Wafer micro crack inspection.	Penetrating light intensity affected by wafer thickness.
3D - Stereo	General 3D dimension check.	Not suitable for high reflective surface. Much complex hardware set-up.
3D – Sheet of light	General 3D surface reconstruction.	Occlusion issue. Not suitable for high reflective surface. Contain uncertainty created by speckle.